X-616-68-171
PREPRINT

NASA TM X- 63206

INTRINSIC MAGNETIC PROPERTIES OF THE LUNAR BODY

KENNETH W. BEHANNON

MAY 1968

GSFC
GODDARD SPACE FLIGHT CENTER
GREENBELT, MARYLAND

INTRINSIC MAGNETIC PROPERTIES OF THE LUNAR BODY

Kenneth W. Behannon
Laboratory for Space Sciences
NASA-Goddard Space Flight Center
Greenbelt, Maryland

May 1968

Extraterrestrial Physics Branch Preprint Series

WORLD DATA CENTER A

Meteorology

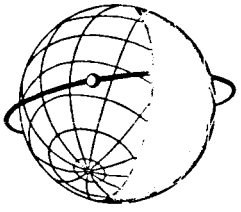

DATA REPORT

METEOROLOGICAL ROCKET NETWORK FIRINGS

June 1967

Volume IV Number 6

CORRESPONDENCE ROUTING SLIP

	Office Symbol	Name (if necessary)		Action
				Approval
1		A & I		Concurrence
				File
2				Information
				Investigate & Advise
3				Note and Forward
				Note and Return
4				Per Request
				Recommendation
5				Coordination
				Signature
6				Reply for Signature of:
7				US:

Remarks:

RE: Trade in Confidence

All Australian documents marked "Trade in Confidence" should have the Distribution Limitation "U.S. Government Agencies Only". Any such document without this limitation should be brought to my attention.

Thank you

From: JLC:jb

Staff Symbol	Name: John L. Christian	Date: 5-22-68

Facility Form 489, Revised July, 1966

APPENDIX A

CHECKLIST OF NASA TECHNICAL THESAURUS CATEGORIES

Aerodynamics

0101	Aerodynamic Characteristics
0102	Aerodynamics of Bodies, Airfoils, Combinations, Protuberances
0103	Internal Flow
0104	Lifting Bodies
0105	Wings, Rotors, Propellers, and Control Surfaces, Aerodynamics

Aircraft

0201	Aeronautics
0202	Aircraft Components and Equipment
0203	Aircraft Noise and Sonic Boom
0204	Aircraft Safety and Landing Devices
0205	Commercial Aircraft (Including Supersonic Transport)
0206	Gliders
0207	Ground Effect Machines
0208	Helicopters
0209	Hypersonic Vehicles
0210	Military Aircraft
0211	Parachutes and Decelerators
0212	STOL/VTOL Aircraft
0213	Inflatable Aircraft and Balloons

Auxiliary Systems

0301	Actuators
0302	Automatic Flight Control
0303	Auxiliary Gas Systems
0304	Auxiliary Gas Turbines
0305	Auxiliary Power Systems
0306	Chemical Batteries
0307	Electric Generators
0308	Energy Conversion Techniques
0309	Fuel Cells
0310	Hydraulic, Pneumatic, and Electrical Systems
0311	Solar Space Power

Biosciences

0401	Aerospace Medicine
0402	Animals
0403	Biochemical Materials (Biochemistry)
0404	Biosciences
0405	Clinical Medicine

0406	Cytology
0407	Exobiology
0408	Microorganisms
0409	Physiological and Psychological Factors
0410	Plants
0411	Psychology
0412	Radiation Effects on Biological Systems
0413	Toxicology

Biotechnology

0501	Bioinstrumentation and Biotelemetry
0502	Crew Training, Safety, and Evaluation
0503	Cybernetics and Bionics
0504	Environmental Control
0505	Food, Water Technology and Waste Disposal
0506	Human Engineering
0507	Life Support Systems
0508	Protective Clothing and Equipment

Chemistry

0601	Chemical Analysis
0602	Chemical Processes and Engineering
0603	General Chemistry
0604	Electrochemistry
0605	Photochemistry and Luminescence

Communications

0701	Communications Equipment
0702	Communications Systems and Techniques
0703	Information Theory
0704	Noise
0705	Radio and Radar
0706	Communications Satellites
0707	Space Communications and Command Systems
0708	Telemetry
0709	Tracking Systems
0710	Wave Propagation

Computers

0801	Computer Hardware
0802	Computer Operation and Programming
0803	Data Processing and Retrieval
0804	Information Retrieval
0805	Computer Simulation

Electronic Equipment

0901	Antennas
0902	Circuitry
0903	Electronic Component Parts
0904	Electrical Equipment
0905	Electronic Equipment
0906	Electronic Test Equipment
0907	Microminiaturization
0908	Semiconductor Devices
0909	Transistors

Electronics

1001	Circuit Theory
1002	Electromagnetic Radiation
1003	Electronics
1004	Feedback and Control Theory
1005	Microelectronics and Microcircuits

Facilities, Research and Support

1101	Airports (Air Facilities)
1102	Ground Support Systems
1103	Handling and Storage Facilities
1104	Launch Facilities
1105	Lunar and Planetary Bases
1106	Research and Support Facilities
1107	Simulators
1108	Test Facilities
1109	Test Ranges
1110	Tracking Stations
1111	Wind Tunnels

Fluid Mechanics

1201	Fluid Amplification and Amplifiers
1202	Fluid Mechanics
1203	Gas Dynamics
1204	Hydrodynamics
1205	Hydrofoils

Geophysics

1301	Lower Atmosphere
1302	Upper Atmosphere
1303	Cartography
1304	Geodesy
1305	Geographical Locations and Geological Formations
1306	Geology
1307	Geomagnetism
1308	Geophysics

1309	Gravitation
1310	Oceanography
1311	Seismology

Instrumentation and Photography

1401	Aerial Photography
1402	Aircraft Instrumentation
1403	Gyroscopes
1404	Infrared and Ultraviolet Devices
1405	Interferometry
1406	Lunar and Space Photography
1407	Measuring Instruments and Calibration
1408	Photography
1409	Pressure and Temperature Measurement
1410	Sensors
1411	Spacecraft Instrumentation
1412	Spectroscopy
1413	Telescopes and Cameras
1414	Transducers

Machine Elements and Processes

1501	Bearings, Seals, Pumps
1502	Handling of Materials
1503	Lubrication, Friction, and Wear
1504	Machine Elements and Processes
1505	Nondestructive Testing
1506	Reliability and Quality Control
1507	Vacuum Technology
1508	Welding and Fabrication

Masers

1601	Masers and Lasers

Materials, Metallic

1701	Alloys
1702	Cermets
1703	Corrosion
1704	Metallic Elements
1705	Metallurgy and Metallography

Materials, Nonmetallic

1801	Ceramic Materials
1802	Coatings and Films
1803	Coolants
1804	Filament Winding
1805	Inorganic Compounds and Ions
1806	Nonmetallic Materials

1807	Minerals and Ores
1808	Nonmetallic Elements
1809	Organic Compounds
1810	Plastics and Elastomers
1811	Polymers
1812	Textiles and Fabrics

Mathematics

1901	Celestial Mechanics
1902	Mathematics
1903	Numerical Analysis
1904	Orbit and Trajectory Calculations
1905	Statistics

Meteorology

2001	Climatology
2002	Meteorological Instruments
2003	Meteorology
2004	Meteorological Satellites

Navigation

2101	Air Traffic Control
2102	Guidance and Control
2103	Navigation
2104	Navigation Instruments

Nuclear Engineering

2201	Nuclear Auxiliary Power and Isotopic Space Power
2202	Nuclear Engineering
2203	Nuclear Instrumentation
2204	Nuclear Reactor Components and Fuels
2205	Nuclear Reactors and Critical Assemblies
2206	Nuclear Rockets
2207	Thermonuclear Devices

Physics, General

2301	Acoustics
2302	Conductivity
2303	Cryogenics
2304	Electricity
2305	Ferroelectricity and Ferromagnetism
2306	Light
2307	Magnetism
2308	Mechanics
2309	Microwaves
2310	Optics
2311	Physics, General
2312	Ultrasonics

Physics, Atomic, Molecular, and Nuclear

2401	Atomic Physics
2403	Elementary Particles
2404	Molecular Physics
2405	Nuclear Physics
2406	Radioisotopes and Stable Isotopes

Physics, Plasma

2501	Plasma Devices
2502	Plasma Physics (Magnetohydrodynamics)

Physics, Solid State

2601	Crystallography and Crystal Structure
2602	Semiconductor Theory and Materials
2603	Solid State Devices
2604	Solid State Physics
2605	Superconductivity

Propellants

2701	Aviation Fuels
2702	Rocket Propellants and Fuels

Propulsion Systems

2801	Aircraft Engines
2802	Auxiliary Propulsion
2803	Electric Propulsion
2804	Liquid Propulsion
2805	Magnetohydrodynamic Propulsion
2806	Ramjet, Turbojet, and Turbofan Engines
2807	Rocket Components
2808	Rocket Control
2809	Rocket Engines
2810	Solid Propulsion

Space Radiation

2901	Cosmic Radiation
2902	Solar Radiation
2903	Space Radiation

Space Sciences

3001	Astronomy
3002	Astrophysics
3003	Cosmology
3004	Lunar Flight and Exploration

3005	Meteors and Meteorites
3006	Orbit and Trajectory Analysis
3007	Planetary Flight and Exploration
3008	Planets
3009	Space Sciences

Space Vehicles

3101	Guided Missiles
3102	Launch Operations
3103	Launch Vehicles
3104	Manned Space Capsules
3105	Reentry Vehicles
3106	Rockets
3107	Satellites
3108	Sounding Rockets and Probes
3109	Space Stations
3110	Space Vehicles

Structural Mechanics

3201	Impact Phenomena
3202	Inflatable Structures
3203	Reinforced Structures
3204	Structural Mechanics
3205	Structural Fatigue

Thermodynamics and Combustion

3301	Combustion
3302	Explosives and Pyrotechnics
3303	Heat Transfer
3304	Thermodynamics
3305	Thermal Protection

General

3401	Defense (Military Science)
3402	Economics and Sociology
3403	History, Law, and Political Science
3404	Industrial Applications and Technology
3405	Information Technology and Documentation
3406	Management
3407	Processes
3408	Properties
3409	Space Programs

POSTABLE TERMS ADDED TO THE THESAURUS AUTHORITY LIST FEB. 27, 1968

PLANETOLOGY

QUARKS

BEAM SPLITTERS

BOEING 747 AIRCRAFT

INTELSAT SATELLITES

DEEP SPACE NETWORK

APOLLO APPLICATIONS PROGRAM

ACTIVATION ANALYSIS

ALKALINE EARTH METALS

ALUMINUM 26

ALUMINUM 27

APOLLO LUNAR SURFACE EXPERIMENTS PACKAGE

ESSA SATELLITES

ESSA 2 SATELLITE

ESSA 3 SATELLITE

HADRONS

IBM 360 COMPUTER

IRAN

JP-5 JET FUEL

LOCAL SCIENTIFIC SURVEY MODULE

NITROGEN PLASMA

RING LASERS

RICCATI EQUATION

SNAP 27

SNAPTRAN REACTOR

[redacted]

PARABALOID MIRRORS -- Deletion

RADIOFREQUENCY INTERFERENCE -- Deletion

FLUID LOGIC

ESSA 1 SATELLITE

SURVEYOR 3 LUNAR PROBE

TAB 200 series not f

Abstract

Preliminary analysis of magnetic measurements by Explorer 35 in lunar orbit suggested an upper limit of 4×10^{20} gauss-cm^3 for the magnetic moment of the moon. A more detailed analysis of a larger body of Explorer 35 data from measurements in the earth's magnetic tail has subsequently been performed. Reversal of the ambient tail field by 180° when the moon and spacecraft traverse the neutral sheet permits a separation of permanent and induced field contributions to the total field observed near the moon. When compared to calculated permanent and induced field effects, the results of this analysis lead to new upper limits of 10^{20} gauss-cm^3 on the lunar magnetic moment and 4γ on the lunar surface field. Limiting the moment induced in the moon by the magnetotail field permits an upper limit of 1.8 to be set on the bulk relative magnetic permeability of the moon.

Introduction

Previous spacecraft measurements in the vicinity of the moon have set upper limits on an intrinsic lunar magnetic field such that if a lunar field exists at all, it is very weak. In 1959 Luna 2 made measurements to within 55 km of the moon's surface (Dolginov et al., 1961), and no lunar associated magnetic field as large as 50-100γ was observed at that altitude. The experimenters set an upper limit of 6×10^{21} gauss-cm^3 on the magnetic moment of the moon.

In 1966 the orbit of Luna 10 carried it to within 350 km of the lunar surface (Dolginov et al., 1966; 1967). The magnetic field measurements obtained by that spacecraft and their interpretation as detection of a pseudo-magnetosphere have been questioned (Ness, 1967). No new limit on the lunar magnetic moment was set by the experimenters. From the measurements reported, however, one may infer an upper limit on the moment of $1\text{-}3 \times 10^{21}$ gauss-cm^3. Neither Luna 2 nor Luna 10 detected a dipole-like variation in the magnetic field measured near the moon.

Lunar Explorer 35 was placed into selenocentric orbit on July 22, 1967 with aposelene = 9388$\pm$100 km, periselene = 2568$\pm$100 km, and period = 11.5 hours. Instrumentation of the Goddard Space Flight Center magnetometer on Explorer 35 and initial results have been previously described (Ness et al., 1967). Subsequently a more detailed study has been made of the interaction of the solar wind with the moon and the resulting perturbation of the interplanetary magnetic field

(Ness et al., 1968). The GSFC experiment makes total vector measurements of the ambient magnetic field at 5.12 second intervals with a sensitivity of $\pm 0.1\gamma$. The initial results showed that the moon does not trap interplanetary field lines to form a lunar magnetosphere. They also enabled the lowering of the upper limit on the magnetic moment of the moon by more than an order of magnitude below the Luna 2 value, to 4×10^{20} gauss-cm^3.

The purpose of this work is to present results of a more detailed study of Explorer 35 data which lead to a still lower upper limit on the lunar magnetic moment and in addition permit an upper limit to be placed on the bulk relative permeability of the lunar body.

Data Analysis

If the moon has a weak permanent magnetic field, it would be highly distorted by the solar wind outside the geomagnetic field. For the detection of the effect of a weak intrinsic lunar field, the best environment is the geomagnetic tail where the ambient field at the lunar orbital distance is known from previous measurements to be steady in magnitude and direction except in the vicinity of the plasma sheet (Behannon, 1968). The moon moves relatively slowly through the tail, so that under conditions of a steady tail field, a lunar field in the magnetotail should be treatable as a static case to a good approximation. The amplitude of the interaction between the medium and the moon should be below the level of detectability of magnetometers currently in use (Sonett and Colburn, 1968).

Figure 1 shows the path of the moon across the earth's tail in solar magnetospheric coordinates as seen from the earth during October 1967. There are periods of time when the diurnal neutral sheet oscillations move the sheet far enough away from the moon so that the field surrounding the moon is characteristically oriented in the solar or antisolar direction and is relatively steady. The first periselene passes on October 17 and 19 occurred during such periods.

When the moon traverses the neutral sheet during passage across the tail, then in principle one can make use of the field reversal across the sheet to distinguish between a permanent lunar field and a field induced in the moon by the tail field. This is because an

induced moment is given by

$$\vec{M}_{induced} = f\left(\mu_m, \frac{R_c}{R_m}\right) \frac{4}{3} \pi R_m^3 \vec{B}_{tail}, \qquad (1)$$

where $\mu_m = \mu/\mu_o$ is the bulk relative permeability of the moon, R_c is the radius of a core region inside of which the temperature is above the Curie point, and R_m is the unit of lunar radius (1738 km). The induced moment is seen to be a function of the volume of the moon and of the inducing tail field as well. Thus, if the magnetotail field above the neutral sheet is $\vec{B}_{T+} = \vec{B}_{tail}$, then the field below the sheet is $\vec{B}_{T-} = -\vec{B}_{tail}$ and the induced moment below the sheet is $\vec{M}_{induced-} = -\vec{M}_{induced+}$.

If the total magnetic moment of the moon above the neutral sheet is given by

$$\vec{M}_+ = \vec{M}_{perm} + \vec{M}_{induced+},$$

where $\vec{M}_{perm}$ is a permanent lunar magnetic moment, then the total moment below the sheet is simply

$$\begin{aligned} \vec{M}_- &= \vec{M}_{perm} + \vec{M}_{induced-} \\ &= \vec{M}_{perm} - \vec{M}_{induced+}. \end{aligned}$$

The permanent and induced moments are then given in terms of the respective total moments by

$$\vec{M}_{perm} = \tfrac{1}{2} (\vec{M}_{+} + \vec{M}_{-}) \tag{2}$$

and

$$|\vec{M}|_{induced} = \tfrac{1}{2}|\vec{M}_{+} - \vec{M}_{-}|. \tag{3}$$

One can see from (2) and (3) that if the total field observed near the moon by the satellite is

$$\vec{B} = \vec{B}_{perm} + \vec{B}_{induced} + \vec{B}_{tail},$$

then it should be possible to separate the various components by utilizing measurements from each side of the field reversal region, realizing that there is a difference in the coordinate system appropriate for identification of the respective components. Since an induced field should be aligned with the tail field, solar ecliptic coordinates are adequate for studying induced field effects. A permanent lunar field, on the other hand, should be fixed relative to the moon, which is rotating. Thus selenographic coordinates, which are fixed to the lunar surface, would be a suitable choice of coordinates for attempting to isolate a permanent field variation.

Using a selected pair of passes near the moon from below and above the neutral sheet, one can calculate from each set of field measurements performed at the same position in the respective coordinate systems the two vectors

$$\vec{B}_{perm} = \tfrac{1}{2} (\vec{B}_{+} + \vec{B}_{-}) \qquad \text{(selenographic)}$$

and

$$\vec{B}_{induced} = \tfrac{1}{2} (\vec{B}_{+} - \vec{B}_{-}) - \vec{B}_{tail} \text{ (solar ecliptic)}.$$

In this way a suite of paired data obtained near the moon can be made to yield the separate influences of both permanent and induced lunar fields as functions of position and distance from the moon. As can be seen from (1), the detection or limiting of an induced field permits a limit to be set on the lunar permeability given a value for R_C, the Curie point radius.

Experimental Observations

The experimental data to be discussed consist of field measurements performed by Explorer 35 during three successive passes of the moon through the geomagnetic tail in August, September and October 1967. No pairs of field measurement sets suitable for the field reversal analysis were found in August due to geomagnetic conditions being disturbed at the beginning of the tail pass (Σ Kp was 23 + on August 18) and the moon being continuously embedded in the plasma sheet near the end of the pass. Figure 2 shows paired data typical of the September tail pass. While the field was relatively steady on September 17 when the moon was below the neutral sheet, large intermittent variations in the field on September 19 when the moon was above the neutral sheet but closer to it limit the usefulness of this pair. Σ Kp was 25 + on September 19 compared to a value of 12- on September 17.

The best pair of measurements obtained from Explorer 35 were on October 17 and 19, around the first periselene passages on each of those days (see Figure 1). Σ Kp ranged from 18 on October 17 down to 9 on October 19. The data are shown in Figure 3. They consist not only of measurements of the field through periselene (marked P) but also through a solar ecliptic azimuth of 360°, which would be a pole of an induced field in the magnetotail. Individual points represent 81.8 second averages of 5.12 second vector measurements performed both below (.) and above (+) the neutral sheet. Even in the case of these

data the observed field was not completely steady. The effects of approximately 20 minute period waves, which have previously been observed in the magnetosphere by Explorer 33 (Behannon, 1968), are seen.

One would expect the reversal of the ambient field to result in antisymmetric trends in the pairs of data curves if the effects of an induced field are observed by the spacecraft. This is weakly suggested by the BX component data. On the other hand, permanent lunar field measurements from different passes should have nearly identical trends if the spacecraft tracks approximately the same path through the lunar field on each of the passes. Equivalently, the subsatellite point must trace out approximately the same path on the lunar surface in each of the passes. A transformation to selenographic coordinates permits one set of data to be shifted relative to the other so that this condition is satisfied if the data sets are not separated in time by more than a few days. The data shown in Figure 3 are in solar ecliptic coordinates with the respective positions of the zeros of selenographic longitude (λ_{SG}) indicated. The perselene distance varied from 817 km on October 17 to 869 km on October 19. A field that varies $\propto R_M^{-3}$ would decrease by 20% in that distance.

The analysis described in the previous section was performed on these data and the respective residual fields are shown in Figure 4. The solid curves, as functions of selenographic longitude, should show

the effects of a permanent field, while the dotted curves, as functions of solar ecliptic azimuth, should reveal any induced field effect. As can be seen, they show that neither a permanent nor an induced field makes a contribution of as much as 1γ to the magnitude of the observed field at the distance of Explorer 35 at periselene, or at an azimuth of 360° in the case of the induced component. A total field residual of 1γ is seen in the permanent field traces at a time which is post-periselene and occurs at a distance from the surface of 886 km. The field magnitude could increase with distance in a dipole field if the spacecraft is moving toward the polar region of the field. The observed peak is more probably the result of superposition of temporal variations occurring in the respective fields which have been summed.

Figures 5 and 6 summarize the total field variations observed by Explorer 35 from August through October for the selenographic longitude range of 0°-140°. The progressive advancement of the periselene point toward 0° is seen in the distance values. Selenographic latitude did not vary by more than 6° at any given longitude throughout the period covered by the data. The periselene distance from the lunar surface varied between 747-886 km during this period. The large degree of variability seen in the data is due at least in part to the close proximity of the moon to the neutral sheet much of the time. No consistent pattern of variation is evident, and no increase in the magnitude larger than approximately $\frac{1}{2}\gamma$ is seen near periselene on those passes where the field is relatively steady, as on September 17 (sequence 77,694) and on September 19 (sequence 79,710).

Table 1 summarizes the conditions of the environment in which the observations shown in Figures 5 and 6 were made. The date and telemetry sequence number of the beginning of each run plotted in the figures is listed in the table. For each of the 12 runs of greater than three hours the average total field magnitude $\bar{F}_{AVG}$ is tabulated, along with the value of Kp corresponding to that time interval and the distance of Explorer 35 from the solar magnetospheric equatorial plane at the beginning of the run. The average total field for all 12 passes was found to be 10.3γ. A magnitude of 9-10γ is predicted for the magnetotail field at 60 R_E from the earth by the tail gradient observations of Explorer 33 (Behannon, 1968; Mihalov et al., 1968).

In Table 2 is shown the average trend of the total field with selenographic longitude found from the data shown in Figures 5 and 6. The 12 passes were summed and averaged at 10° intervals of longitude from 130° to 0°, giving the 14 values of average magnitude $\bar{F}_{AVE}$. The average selenocentric distance of Explorer 35 in lunar radii corresponding to each magnitude average is also given. As can be seen the standard deviation of the average total field was found to be only $\pm$ 0.2γ for the 130° range of longitude although the average distance varied by 0.5 R_M.

The total field data also can be summarized in terms of solar ecliptic azimuth. Figure 7 represents a graphical summary for five of the passes near the moon in October. Again the temporal variability is evident, but the data from October 17 (sequence 108,681) and

October 19 (sequences 111,220 and 111,729) show little variation through either periselene or $\phi_{SSE} = 0^{o}$. An effect of approximately 1γ would be expected at 0^{o} for an induced moment of 1×10^{20} gauss-cm^3. This is illustrated in Figure 8, where the average tail field of 9γ and an induced moment of 1×10^{20} were used to compute the effect of an induced field along the actual trajectory of Explorer 35 in a steady ambient field of 9γ.

An induced field effect may be calculated at each point in the orbit using

$$B_R = B_T \cos\theta + 2 M_I \cos\theta/R^3$$

and

$$B_\theta = B_T \sin\theta + M_I \sin\theta/R^3 ,$$

where M_I is the magnitude of the induced moment, R is the selenocentric distance to the point, and θ is the angle between the tail field vector and the radius vector to the point.
In Figure 8 the theoretical field is superimposed as a solid curve on the measured total field and component data from the first periselene pass on October 19. Even with the wave fluctuations in the field it is clear that no regular variation larger than one due to an induced moment of 1×10^{20} gauss-cm^3 is seen in the field observed by the spacecraft.

Interpretation of Results

With these more detailed studies of Explorer 35 measurements near the moon, one is able to set upper limits on the lunar magnetic moment and surface field magnitude that are lower than previous estimates. Table 3 shows the permanent dipole field that would be observed at a periselene distance of 1.4 R_M (~700 km) for different values of the dipole moment magnitude M and equatorial surface field magnitude B_{eq}. For each value of the moment and surface field the table gives the corresponding magnitude of the lunar field at the spacecraft at the given periselene distance if the satellite is over the pole, at 45^o from the pole, or at the lunar magnetic equator. At the maximum periselene distance observed during August-September 1967 (approximately 200 km further from the surface), the field magnitudes that would be observed would be 25% less than the values listed in Table 3.

The most difficult situation to detect from an equatorial orbit would be one in which a permanent magnetic moment would be normal to the ecliptic plane. However, the total field values in the 90^o column in Table 3 show that even in that most obscure case, the field due to a moment $>10^{20}$ should be observable. It can be seen from the table that if no permanent field variations larger than 1γ are detected, then the upper limit on a lunar dipole moment must be of the order of 1×10^{20} gauss-cm^3 with an equatorial surface field no greater than approximately 2γ.

The tests for an induced field effect show that if an induced component is present in the Explorer 35 data through periselene and through an azimuth of 360^{o}, then it is less than 1γ in magnitude also. The comparison with a computed field variation in Figure 8 further shows that if a magnetic moment is induced in the moon, it must be limited to $\leq 1 \times 10^{20}$ gauss-cm^3 as well.

When the magnitude of the inducing tail field is considered along with the upper limit on the induced moment, one can estimate an upper limit on the bulk magnetic permeability of the lunar material. The family of curves shown in Figure 9 relate induced magnetic moment to permeability for a range of values of R_1/R_M, the relative cavity radius, in a spherical shell of permeable material (Jackson, 1962). If one assumes a homogeneous solid moon (R_C=0) so that the equation for magnetic moment given in Figure 9 is valid, then a unique solution for μ_m, the relative permeability, is possible. For an inducing field of 9γ, corresponding to the average tail field magnitude on October 19, and an upper limit on the induced moment of 1×10^{20} gauss-cm^3, an upper limit of 1.8 is obtained for μ_m.

The limit of 1.8 can be compared to values found in the laboratory for various materials which have been suggested for the composition of lunar rocks. It must be remembered that laboratory measurements are performed at temperatures well below the Curie point, since as a material is heated to that temperature the susceptibility goes to zero. A limited number of measurements have been made on chondritic meteorites.

Fensler et al.(1962) found D. C. permeabilities of 1.20 and 2.04 for the Leedy and Plainview meteorites. In a survey of 79 chondrites, Pochtarev and Gus'kova (1962) found values of χ ranging from 0.0032 to 0.220 cgs units. Since

$$\mu/\mu_o = 1 + 4\pi\chi ,$$

one finds that the relative permeabilities of those samples ranged from 1.04 to 3.76. In addition, 16% had permeabilities larger than 1.8. Values for achondrites and eucrites surveyed ranged from 1.0025 to 1.25.

Measurements of susceptibility of common earth rocks (Grant and West, 1965; Clark, 1966) lead to relative permeability values that fall on or below an average of 1.01 for basalt. This is due to a tendency for magnetite to concentrate in mafic rocks, resulting in a higher magnetic susceptibility in these rocks than in more silicic ones. Thus the upper limit set by Explorer 35 on the bulk relative permeability of the lunar body is in the lower 1/3 of the range of measured values for chondritic meteorites and larger than values measured for achondrites and eucrites, as well as those found for terrestrial rocks.

If the Curie point radius for the moon is in fact large, it can be seen from Figure 9 that if $R_C=R_1$ and the magnetic moment is as large as 10^{20} gauss-cm^3 then μ_m could be a large number. However, the

preceding discussion of laboratory measurements of μ_m suggests that the bulk relative magnetic permeability of the moon is probably no larger than the upper limit that was computed for the case of $R_C=0$. This conclusion is supported by the results of the magnet experiments on Surveyors 5, 6 and 7. Those results were consistent with a basaltic structure for the moon's surface at the sites tested (de Wys, 1967,1968).

The question of the value of R_C will remain indeterminate until sufficient measurements are performed on the moon to establish a reliable average value of μ_m for the moon and the induced moment is determined more precisely. If the lunar magnetic permeability is as low as has been measured for terrestrial rocks, even if the moon is solid Figure 9 shows that the moment induced in the moon by the tail field would be at least an order of magnitude lower than the upper limit set by Explorer 35 measurements.

Summary

Measurements obtained in the vicinity of the moon by Luna 2 established an upper limit of 6×10^{21} gauss-cm^3 on the magnetic moment of the moon. Data from Luna 10, the first spacecraft to orbit the moon, suggested a slightly lower moment of $1\text{-}3 \times 10^{21}$ gauss-cm^3. While not finding a dipole-like variation in the Luna 10 measurements near the moon, the magnetic field experimenters did claim to observe a significant excess of the near-lunar field over the undisturbed interplanetary field (Dolginov et al., 1966). However, they state that for the Luna 10 observations to be consistent with a static magnetization of lunar rocks, those rocks would have to have a magnetic permeability of 0.5. The interpretation of the Luna 10 magnetic measurements has been questioned by Ness (1967).

Measurements by the more sensitive GSFC magnetometer onboard Explorer 35 reveal no lunar field of the magnitude observed by Lunar 10 and reduce the upper limit on the lunar magnetic moment to 10^{20} gauss-cm^3. This corresponds, in the case of a permanent dipole field, to an equatorial surface field of no greater than approximately 2γ (and a field no larger than 4γ anywhere on the lunar surface).

Limits of 1×10^{20} gauss-cm^3 on each of the respective moments permit a total magnetic moment in the magnetotail as large as 2×10^{20} for the case in which the two moments are parallel and in the same direction. However, since the search for an induced moment should have detected that larger effect, it is not likely that such an alignment

ever occurs and hence the upper limit on the total moment is also probably of the order of 1×10^{20} gauss-cm^3.

The upper limit on the magnetic moment along with the average magnitude of the earth's tail field permit an upper limit of 1.8 to be set on the bulk relative magnetic permeability of the moon if a solid, homogeneous moon is assumed. Laboratory measurements and Surveyor magnet results suggest that the magnetic permeability is probably not larger than that value, even if the moon's core is not solid. A magnetic permeability on the lower edge of or below the range of values found in the laboratory for chondritic meteorites suggests that the moon is not predominantly composed of cold chondritic material. It could be composed of warm chondritic material but then there would be other detectable effects such as those due to conductivity, and no effects of that nature have been found (Ness, 1968).

Failure to detect a lunar field effect with the Explorer 35 instrument reinforces the conclusion that the bulk of the moon did not cool through its Curie point at some past time in a strong uniform magnetic field, since a relative strong and stable remanence would have been acquired and should have been observed.

Acknowledgements

I am indebted to Dr. N. F. Ness for his many suggestions and continuous support throughout this work. Discussions with Dr. H. E. Taylor, the analysis assistance of Mr. H. E. Haney and Mr. W. H. Mish, and the engineering contributions of Mr. C. S. Scearce and Dr. S. C. Cantarano to the Explorer 35 experiment are also appreciated.

References

Behannon, K. W., Mapping of the Earth's Bow Shock and Magnetic Tail by Explorer 33, J. Geophys. Res., 73, 907-930, 1968.

de Wys, J. N., Lunar Surface Electromagnetic Properties, Surveyor V, A Preliminary Report, NASA SP-163, 133-154, Scientific and Technical Information Division, National Aeronautics and Space Administration, Washington, D.C., December 1967.

de Wys, J. N. Results and Implications of Magnet Experiments on Surveyor 5, 6, and 7 Spacecrafts, Trans. Am. Geophys. Union, 49, 249, 1968.

Dolginov, Sh. Sh., Ye. G. Yeroshenko, L. N. Zhuzgov, and N. V. Pushkov, Investigation of the Magnetic Field of the Moon, Geomagnetism and Aeronomy, 1, 18-25, 1961.

Dolginov, Sh. Sh., Ye. G. Yeroshenko, L. N. Zhuzgov and N. V. Pushkov, Measurements of the Magnetic Field in the Vicinity of the Moon on the AMS Luna 10, Dokl. Akad. Nauk, SSSR, 170, 574-577, 1966 (in Russian).

Dolginov, Sh. Sh., Ye. G. Yeroshenko, L. N. Zhuzgov, and I. A. Zhulin, Possible Interpretation of the Results of Measurements in the Near Lunar Satellite AMS Luna 10, Geomagetizm i Aeronomiya, 7, 436-441, 1967 (in Russian).

Fensler, W. E., E. F. Knott, A. Olte, and K. M. Siegel, The Electromagnetic Parameters of Selected Terrestrial and Extraterrestrial Rocks and Glasses, in The Moon, edited by Z. Kopal and Z. K. Mikhailov, 545-565, Academic Press, New York, 1962.

Grant, F. S. and G. F. West, Interpretation Theory in Applied Geophysics, 355-381, McGraw-Hill, New York, 1965.

Jackson, J. D., Classical Electrodynamics, 162-164, John Wiley and Sons, New York, 1962.

Lindsey, D. H., G. E. Andreasen and J. R. Balsley , Magnetic Properties of Rocks and Minerals, in Handbook of Physical Constants, edited by S. P. Clark, Jr., 543-552, The Geological Society of America Inc., New York, 1966.

Mihalov, J. D., D. S. Colburn, R. G. Currie, and C. P. Sonett, Configuration and Reconnection of the Geomagnetic Tail, J. Geophys. Res., 73, 943-959, 1968.

Ness, N. F., Remarks on the Interpretation of Luna 10 Magnetometer Results, Geomagnetizm i Aeronomiya, 7, 431-435, 1967 (in Russian).

Ness, N. F., Electrical Conductivity of the Moon, Trans. Am. Geophys. Union, 49, 242, 1968.

Ness, N. F., K. W. Behannon, C. S. Scearce and S. C. Cantarano, Early Results from the Magnetic Field Experiment on Lunar Explorer 35, J. Geophys. Res., 72, 5769-5778, 1967.

Ness, N. F., K. W. Behannon, H. E. Taylor and Y. C. Whang, Perturbations of the Interplanetary Magnetic Field by the Lunar Wake, J. Geophys. Res., 73, June 1968.

Po[illegible], V. I. and Ye. G. Gus'kova, The Magnetic Properties of Meteorites, Geomagnetism and Aeronomy, 2, 626-634, 1962.

Sonett, C. P. and D. S. Colburn, Interaction of the Moon with the Geomagnetic Tail Field, Trans. Am. Geophys. Union, 49, 242, 1968.

TABLE 1

AVERAGE TAIL FIELD MAGNITUDE SUMMARY

	SEQ	$\bar{F}_{AVG}(\gamma)$	Kp	$Z_{SM}(R_E)$
18 Aug 1967	45743	13.5	3	-15.6
19 Aug	46752	12.5	2-	-9.3
19 Aug	47253	12.0	3	-5.5
17 Sept	77195	7.8	2	-11.7
17 Sept	77694	10.2	2-	-9.1
18 Sept	78709	12.5	3-	-3.8
19 Sept	79710	10.0	3+	+3.3
16 Oct	108133	9.2	0+	-14.8
17 Oct	108641	7.7	1	-5.2
17 Oct	109140	10.6	2	-8.0
19 Oct	111144	9.2	0+	+6.2
19 Oct	111643	8.1	1	+4.8
	AVERAGE	= 10.3γ		

TABLE 2

AVERAGE FIELD MAGNITUDE VARIATION WITH

SELENOGRAPHIC LONGITUDE

λ_{SG} (deg)	$\overline{F}_{AVE}$ (γ)	$DIST_{AVE}$ (R_M)
130	10.5	2.0
120	10.5	1.8
110	10.5	1.7
100	10.7	1.5
90	10.7	1.5
80	10.3	1.5
70	10.3	1.5
60	10.2	1.5
50	10.1	1.6
40	10.3	1.6
30	10.1	1.7
20	10.2	1.8
10	10.1	1.9
0	10.1	2.0

AVERAGE FIELD MAGNITUDE = 10.3γ

STANDARD DEVIATION OF FIELD = $\pm$0.2γ

TABLE 3

PERMANENT LUNAR DIPOLE FIELD
at R=1.4 R_M

$M = B_{eq} \; R_M^3$ $\qquad |\vec{B}| = \sqrt{B_R^2 + B_\theta^2}$ $\qquad B_R = \frac{2M \cos\theta}{R^3}$ $\qquad B_\theta = \frac{M \sin\theta}{R^3}$

M	B_{eq}	$\lvert\vec{B}\rvert$*		
		$\theta = 0^\circ$ (POLE)	45°	90° (EQUATOR)
4.2×10^{20} cgs	8 γ	5.8 γ	4.6 γ	2.9 γ
3.2×10^{20}	6	4.4	3.4	2.2
2.1×10^{20}	4	2.9	2.3	1.4
1.0×10^{20}	2	1.4	0.9	0.7
0.5×10^{20}	1	0.7	0.6	0.4

* $|\vec{B}|_{1.5\ R_M} = 0.75\ |\vec{B}|_{1.4\ R_M}$

FIGURE CAPTIONS

Figure 1 Variation of the distance (Z_{SM}) of the moon from the solar magnetospheric equatorial ($Z_{SM}=0$) plane in units of R_E (earth radii) during the October 1967 pass of the moon across the geomagnetic tail. Periselene points (P) for Explorer 35 in lunar orbit are shown. Heavy shading along the trajectory indicates intervals when depressed field magnitude was observed, with positions at which temporary and final neutral sheet traversals occurred also marked (R).

Figure 2 Paired GSFC magnetic field data from Explorer 35 passes near the moon on September 17 and 19, 1967. Solar ecliptic component measurements of the vector field (in gammas) both below (.) and above (+) the neutral sheet of the geomagnetic tail are shown as functions of selenocentric solar ecliptic azimuth (ϕ_{SSE}), selenocentric distance of the spacecraft in units of R_M (lunar radii), and relative telemetry sequence number. Approximately 190 minutes of data are shown.

Figure 3 Paired GSFC magnetic field data from Explorer 35 passes near the moon on October 17 and 19, 1967. These measurements together with those shown in Figure 2, demonstrate the continuous absence of a large lunar field effect in a relatively steady magnetotail field.

Figure 4 Solar ecliptic component residuals near the moon obtained from analysis of October 17 and 19 data. These curves show

that both permanent and induced lunar field effects at the spacecraft are less than $\pm\frac{1}{2}\gamma$ at periselene (P).

Figure 5 Total magnetic field magnitudes ($\bar{F}$) on six periselene passes during August 18 to September 18, 1967 as functions of selenographic longitude (λ_{SG}). Selenocentric distance in units of R_M is given with each curve. No recurrent pattern of variation in field magnitude was observed.

Figure 6 Total magnetic field magnitudes measured on six passes during the period September 19 to October 19, 1967. As in Figure 5, no persistent variation with seleographic longitude that could be attributed to a dipole or remanent permanent lunar field is seen in the data.

Figure 7 Total magnetic field magnitudes observed by Explorer 35 during five passes near the moon in October 1967 as functions of selenocentric solar ecliptic azimuth (ϕ_{SSE}) and distance in units of lunar radii. Distance (Z_{SM}) from the solar magnetospheric equatorial plane is given for $\phi_{SSE}=0^{o}$. In this case no regular variation with solar ecliptic azimuth is seen.

Figure 8 Measured total field and solar ecliptic component data for the period 0830-1140 UT, October 19 with calculated induced field (for the case of an unaberrated tail) superimposed. A gradual increase is seen in the measured field around an azimuth of 360^{o}, but a variation with the form of the computed induced field is not seen. The averages of the BX and BY

components during this period give an aberration angle for the magnetotail of $\sim 6^{o}$ (corresponding to a solar wind velocity of ~300 km/sec).

Figure 9 Induced magnetic moment (M) as a function of magnetic susceptibility (μ_m-1), for inducing tail field magnitudes (B_T) of 10 and 15γ. Relative equatorial surface field magnitude corresponding to a given induced moment is shown on the right-hand ordinate. The formulation for computing the induced moment for a solid, homogeneous moon is given.

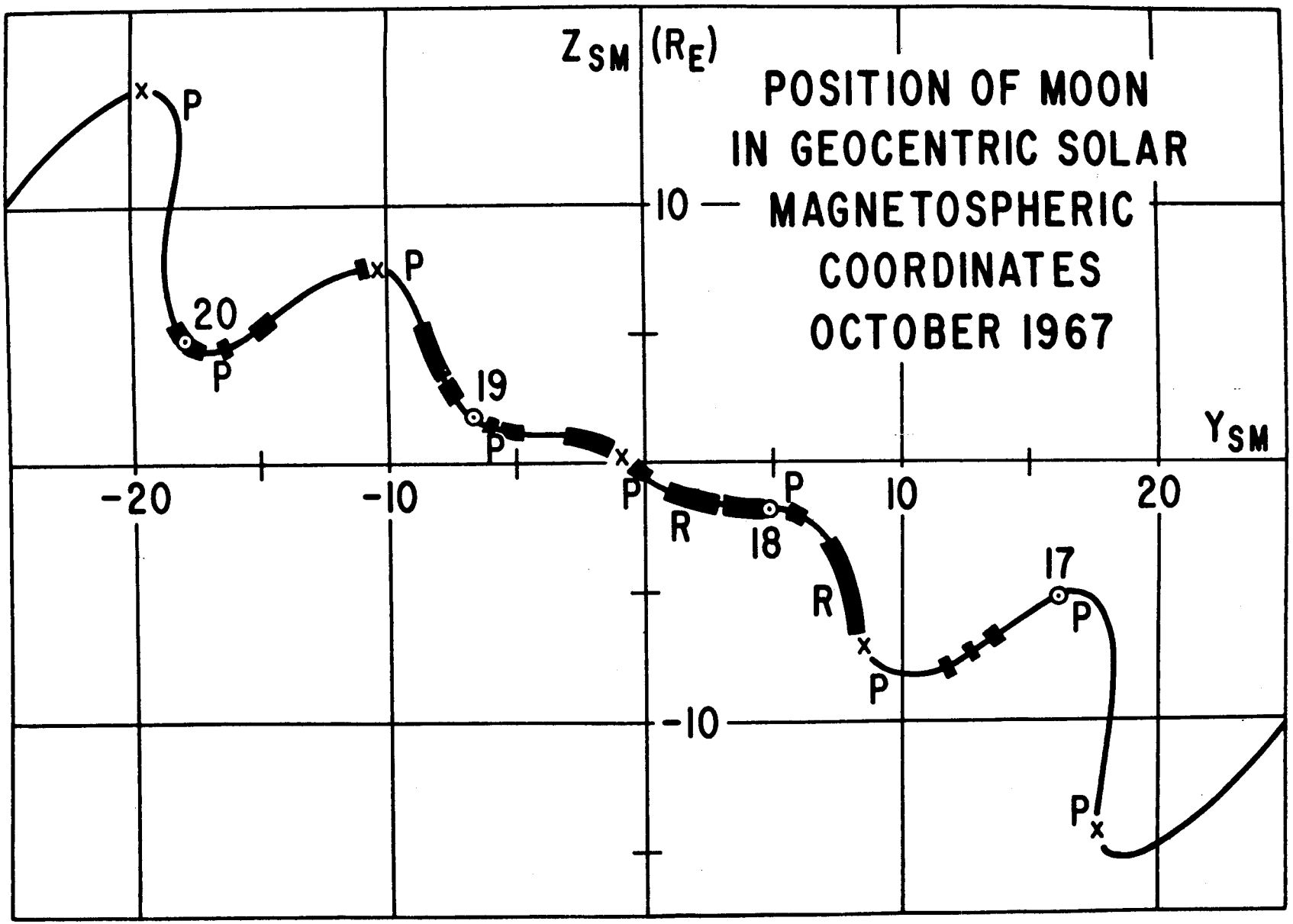
Z SM (R E)
POSITION OF MOON
IN GEOCENTRIC SOLAR
MAGNETOSPHERIC
COORDINATES
OCTOBER 1967
Y SM
10
-10
-20
-10
10
20
20
19
18
17
P
R
x

FIGURE 1

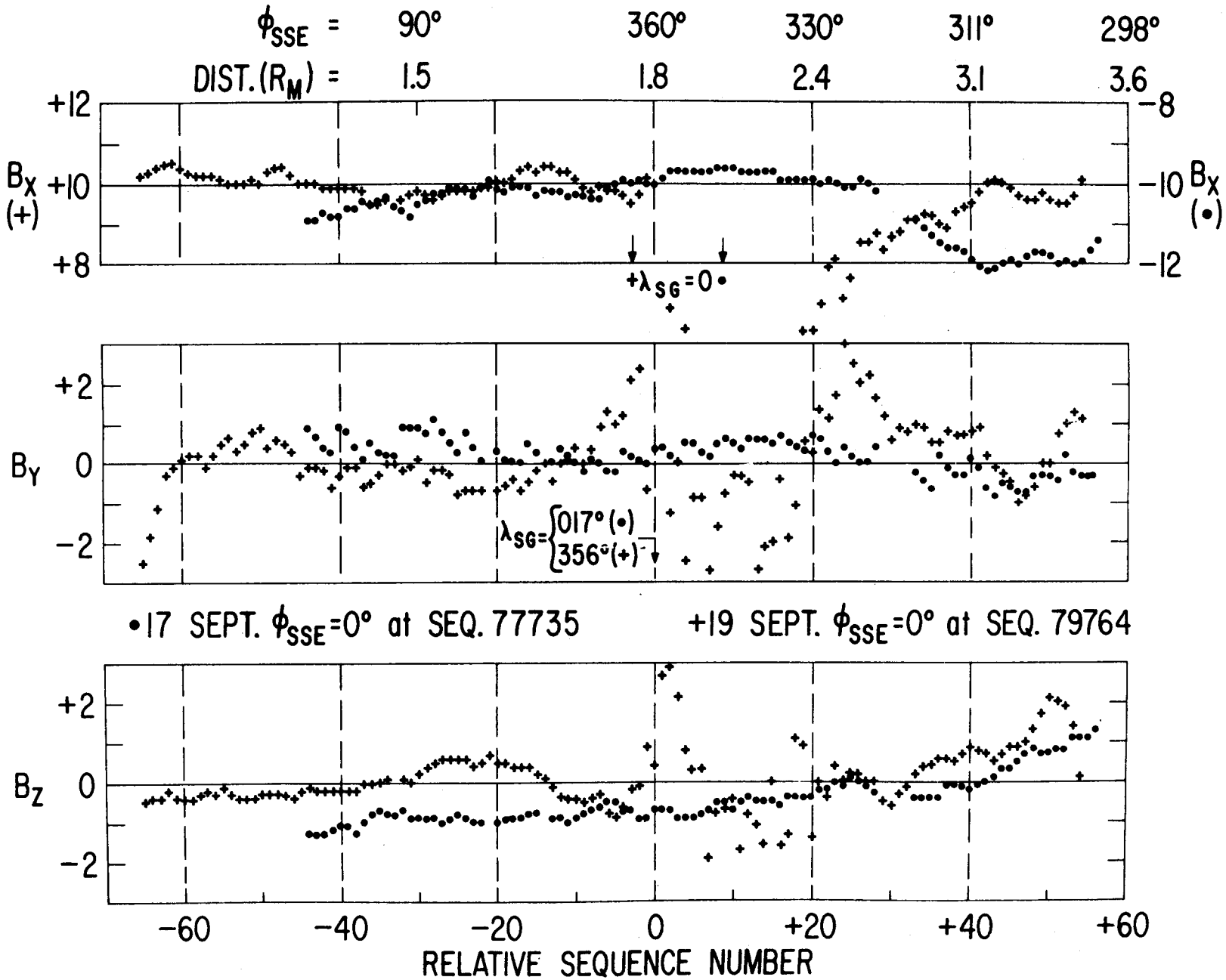
ϕ_{SSE} = 90° 360° 330° 311° 298°
DIST.(R_M) = 1.5 1.8 2.4 3.1 3.6
+12
+10
+8
B_X (+)
−8
−10
−12
B_X (•)
$+\lambda_{SG}=0$•
+2
0
−2
B_Y
λ_{SG} = {017° (•) 356° (+)
•17 SEPT. ϕ_{SSE}=0° at SEQ. 77735
+19 SEPT. ϕ_{SSE}=0° at SEQ. 79764
+2
0
−2
B_Z
−60 −40 −20 0 +20 +40 +60
RELATIVE SEQUENCE NUMBER

FIGURE 2

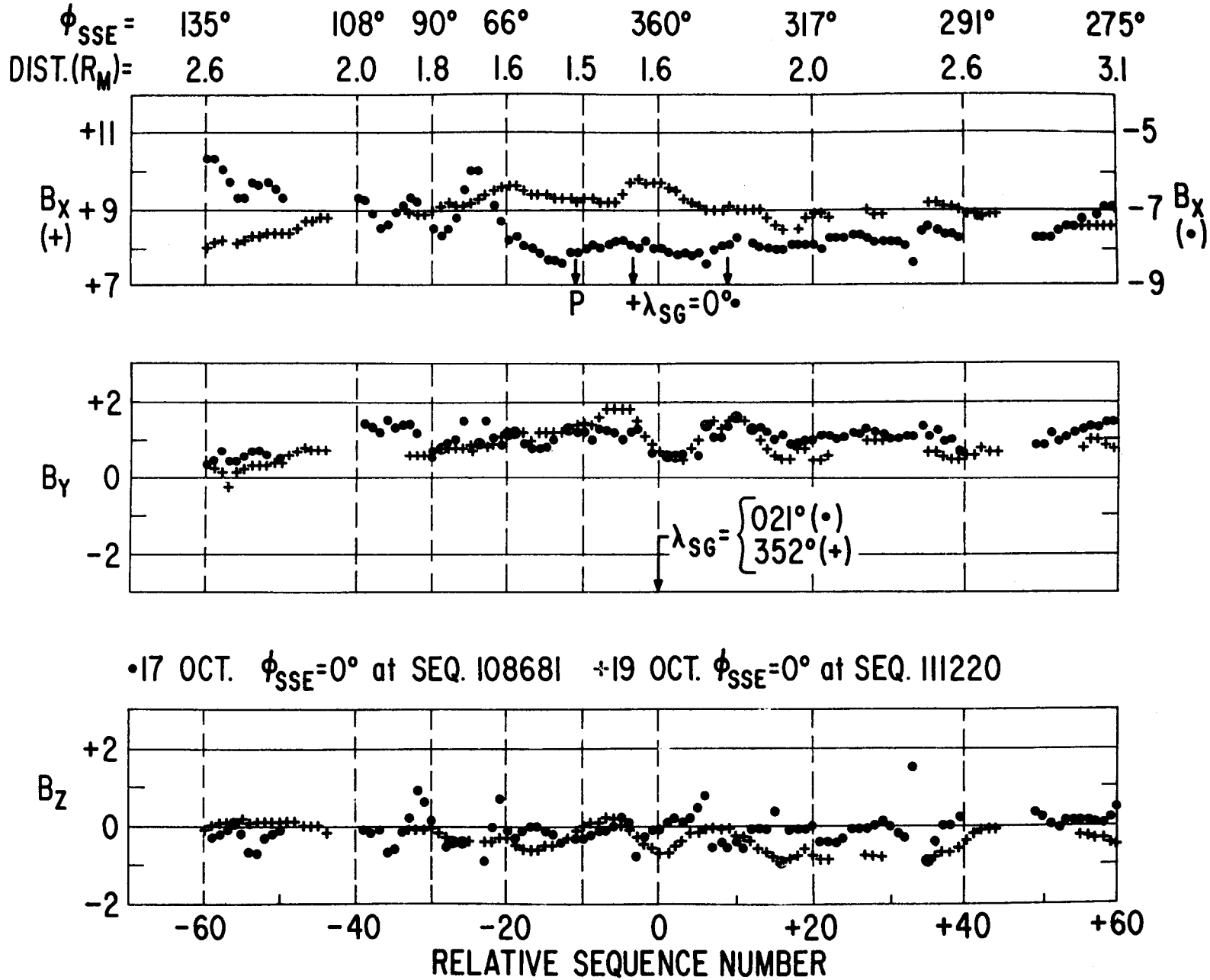
ϕ_{SSE} = 135° 108° 90° 66° 360° 317° 291° 275°
DIST.(R_M)= 2.6 2.0 1.8 1.6 1.5 1.6 2.0 2.6 3.1
+11
B_X (+) +9
+7
-5
-7 B_X (•)
-9
P
$+\lambda_{SG}$=0°
+2
B_Y 0
-2
λ_{SG}= 021°(•) 352°(+)
•17 OCT. ϕ_{SSE}=0° at SEQ. 108681 +19 OCT. ϕ_{SSE}=0° at SEQ. 111220
+2
B_Z 0
-2
-60 -40 -20 0 +20 +40 +60
RELATIVE SEQUENCE NUMBER

FIGURE 3

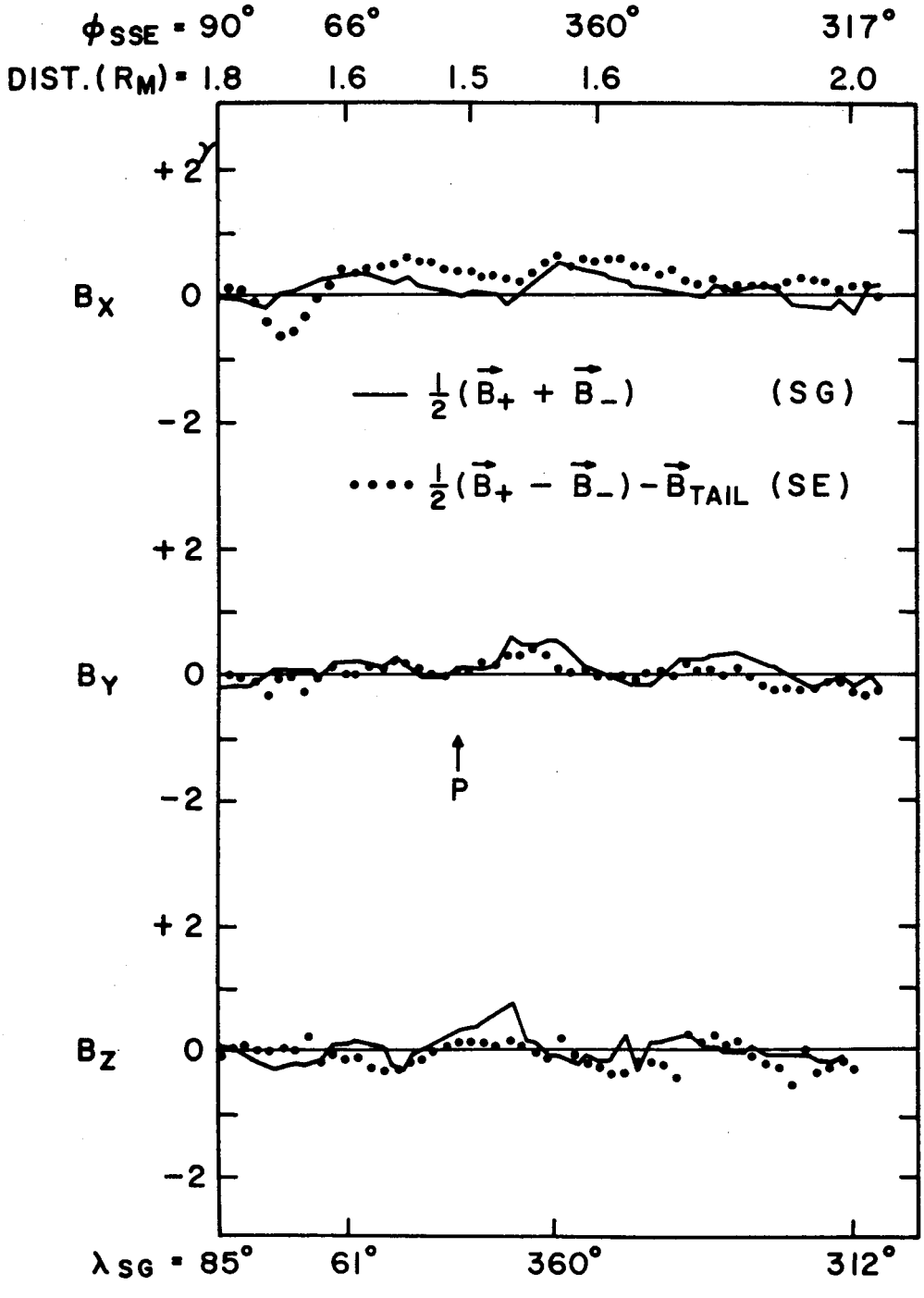

OCTOBER RESIDUAL FIELDS

FIGURE 4

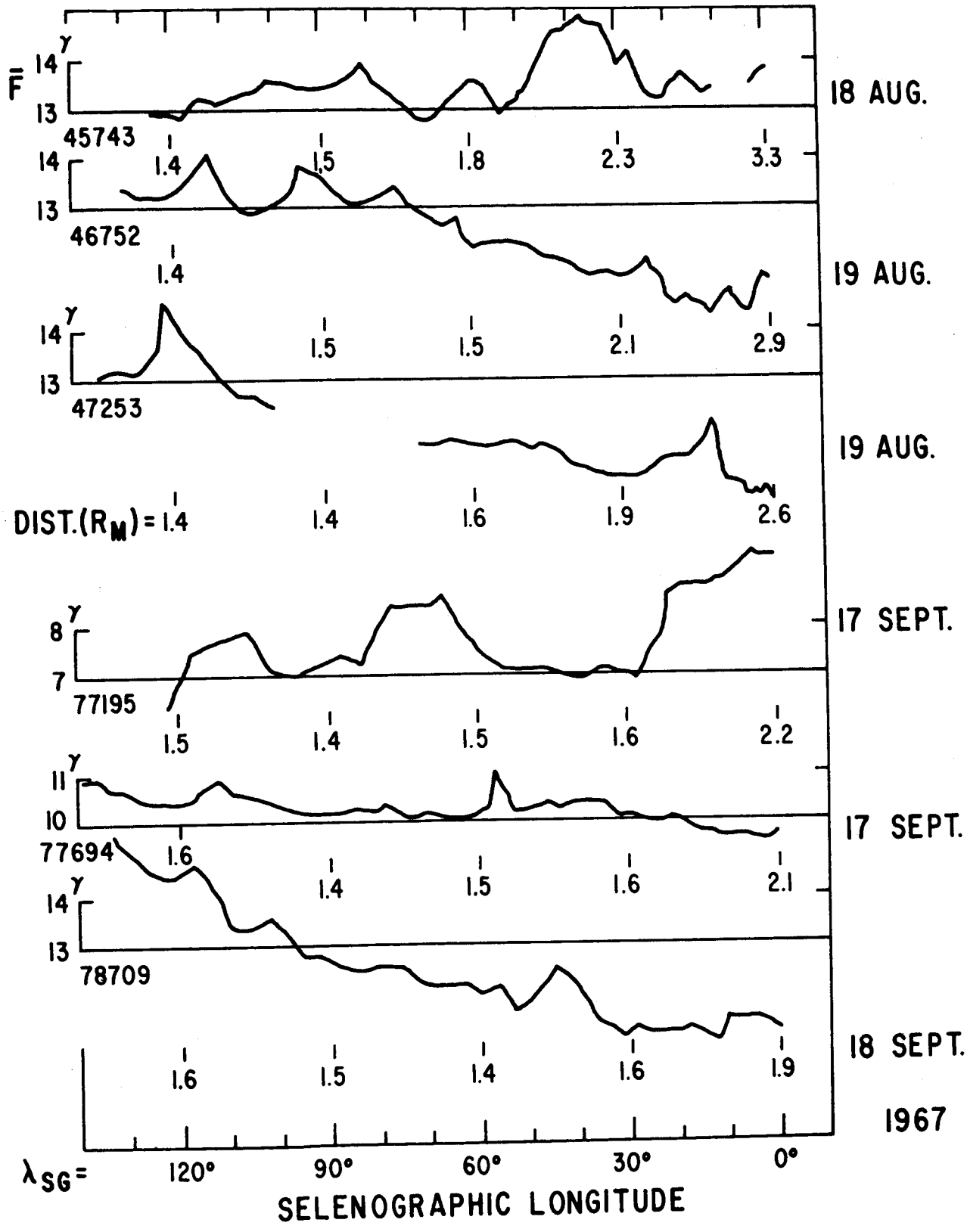
F
γ
14
13
45743
1.4
1.5
1.8
2.3
3.3
18 AUG.
46752
1.4
19 AUG.
47253
1.5
1.5
2.1
2.9
19 AUG.
DIST.(R_M) = 1.4
1.4
1.6
1.9
2.6
8
7
77195
1.5
1.4
1.5
1.6
2.2
17 SEPT.
11
10
77694
1.6
1.4
1.5
1.6
2.1
17 SEPT.
78709
1.6
1.5
1.4
1.6
1.9
18 SEPT.
1967
λ_SG = 120° 90° 60° 30° 0°
SELENOGRAPHIC LONGITUDE

FIGURE 5

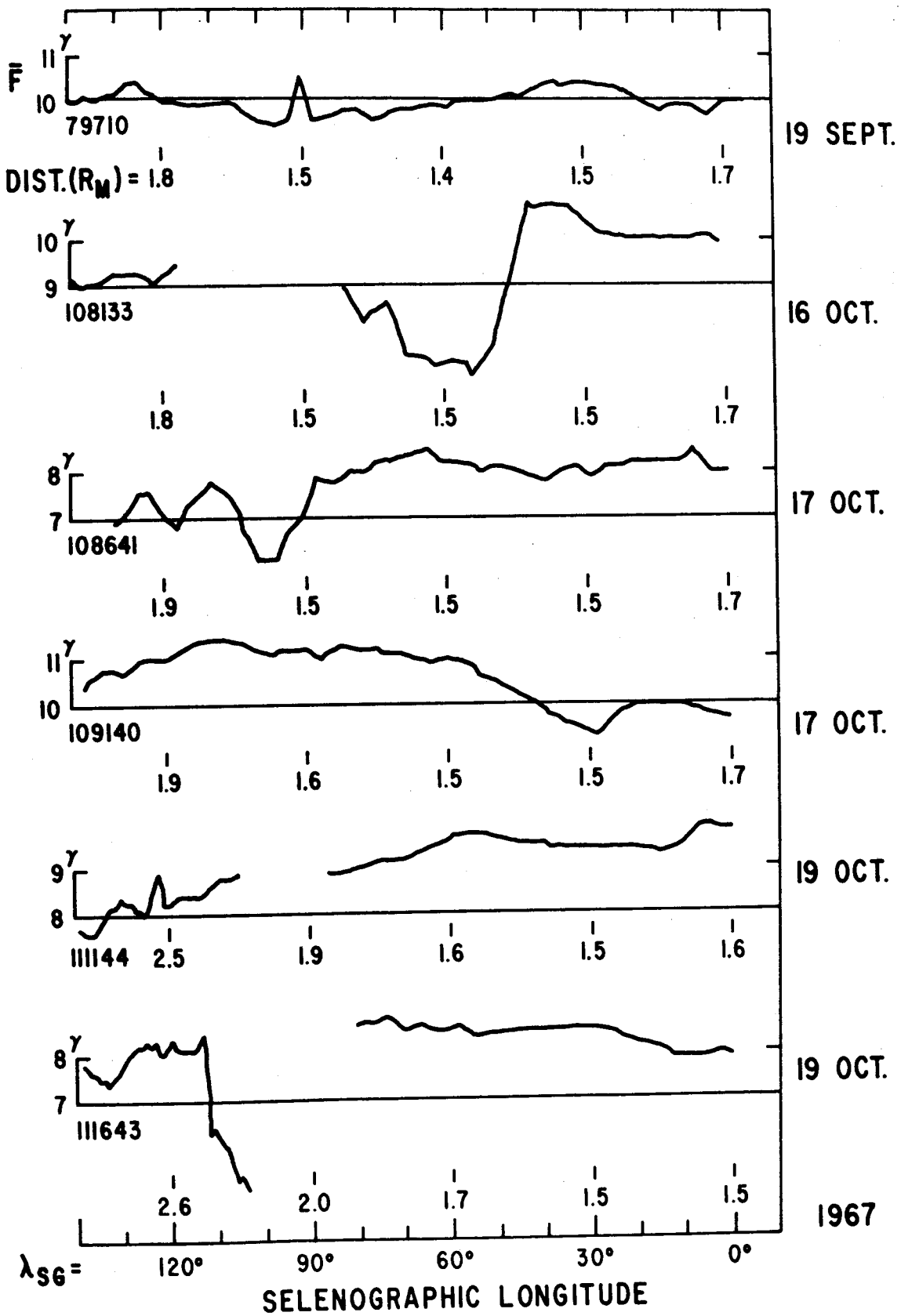
F̄
11γ
10
79710
19 SEPT.
DIST.(R_M) = 1.8 1.5 1.4 1.5 1.7
10γ
9
108133
16 OCT.
1.8 1.5 1.5 1.5 1.7
8γ
7
108641
17 OCT.
1.9 1.5 1.5 1.5 1.7
11γ
10
109140
17 OCT.
1.9 1.6 1.5 1.5 1.7
9γ
8
111144 2.5 1.9 1.6 1.5 1.6
19 OCT.
8γ
7
111643
19 OCT.
2.6 2.0 1.7 1.5 1.5
1967
λ_SG = 120° 90° 60° 30° 0°
SELENOGRAPHIC LONGITUDE

FIGURE 6

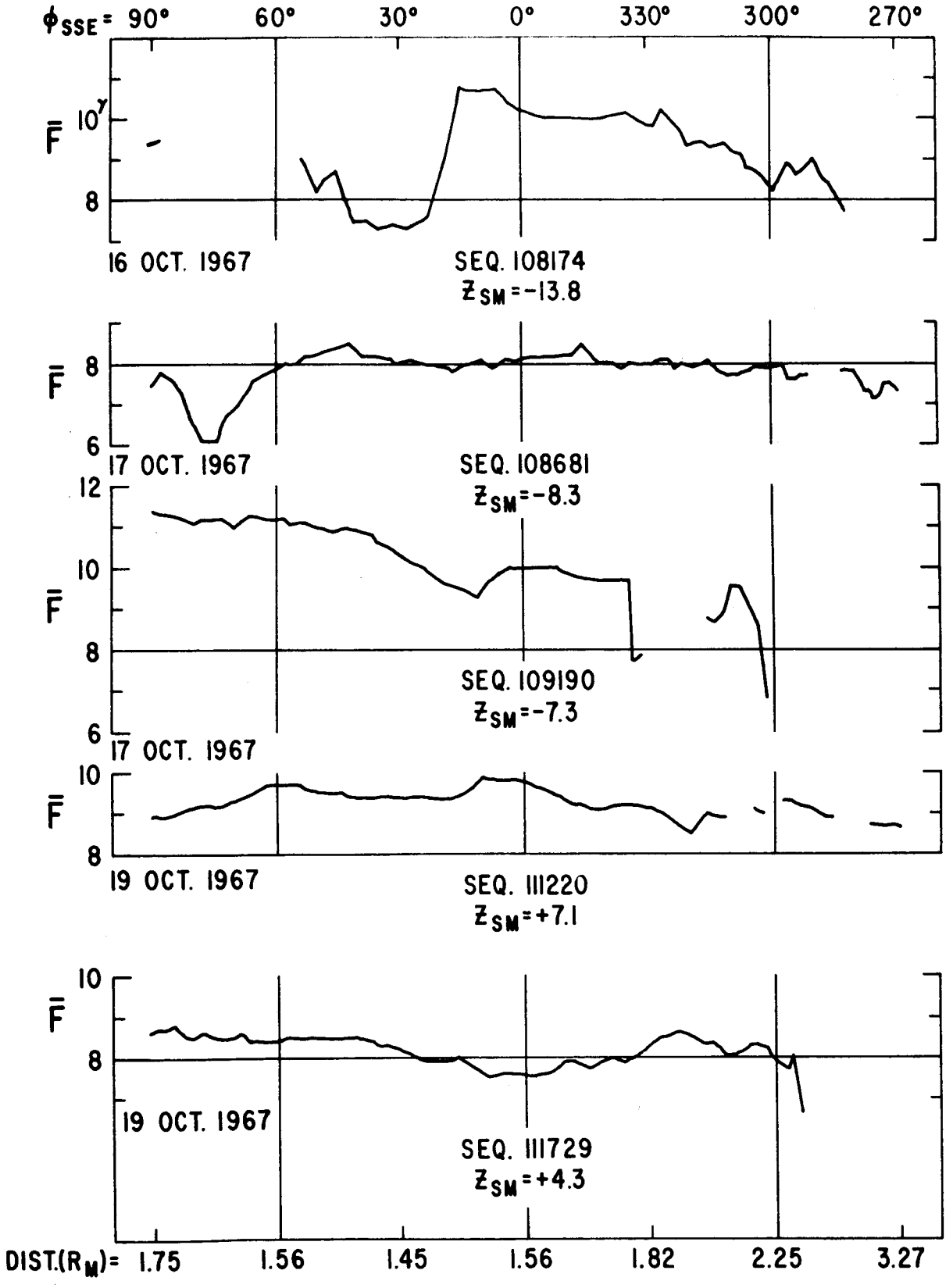
ϕ_{SSE} = 90° 60° 30° 0° 330° 300° 270°
$\bar{F}$ 10^{γ}
8
16 OCT. 1967
SEQ. 108174
Z_{SM} = -13.8
$\bar{F}$ 8 6
17 OCT. 1967
SEQ. 108681
Z_{SM} = -8.3
$\bar{F}$ 12 10 8 6
SEQ. 109190
Z_{SM} = -7.3
17 OCT. 1967
$\bar{F}$ 10 8
19 OCT. 1967
SEQ. 111220
Z_{SM} = +7.1
$\bar{F}$ 10 8
19 OCT. 1967
SEQ. 111729
Z_{SM} = +4.3
DIST.(R_M) = 1.75 1.56 1.45 1.56 1.82 2.25 3.27

FIGURE 7

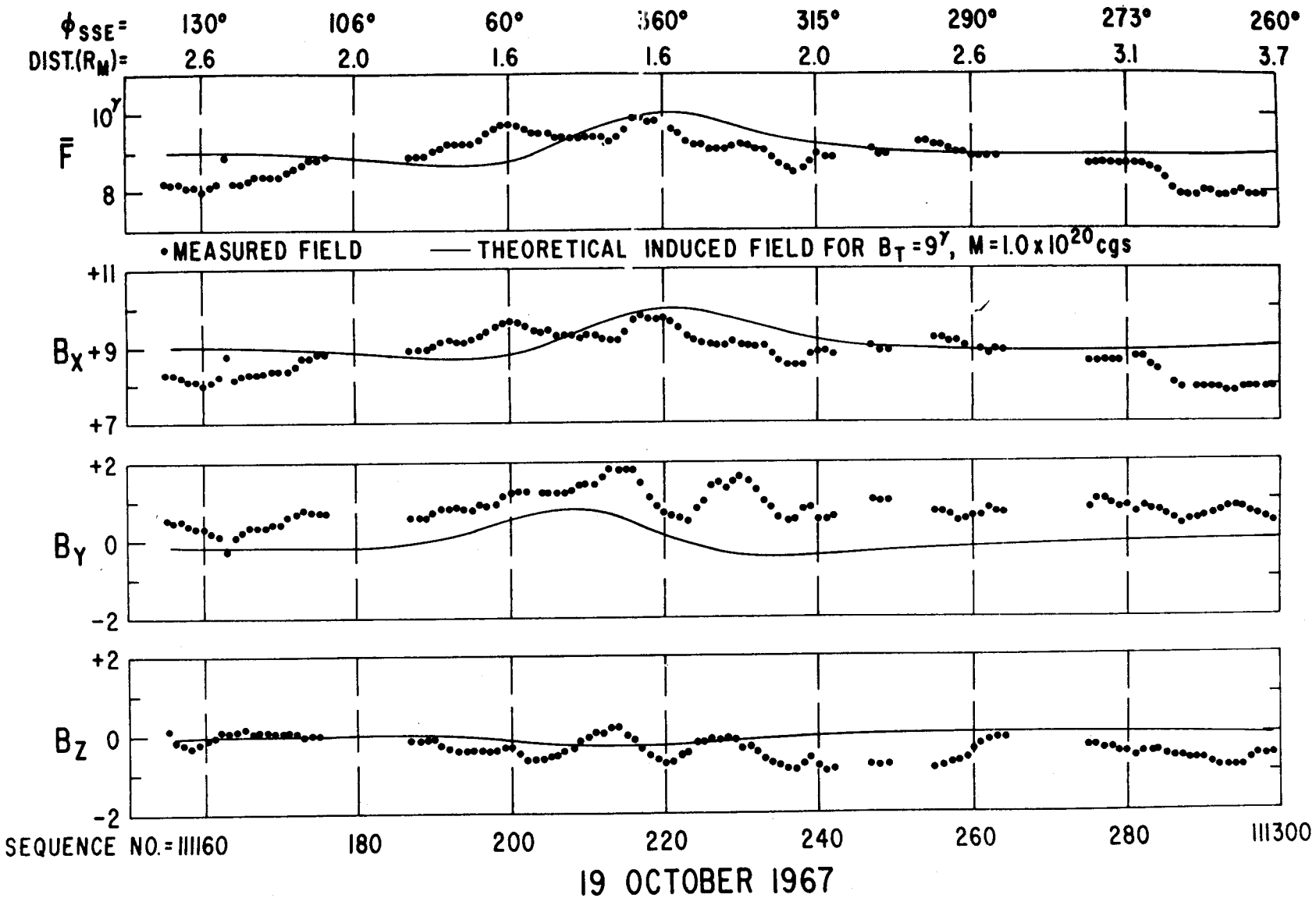
ϕ_{SSE}= 130° 106° 60° 360° 315° 290° 273° 260°
DIST.(R_M)= 2.6 2.0 1.6 1.6 2.0 2.6 3.1 3.7
$\bar{F}$
10γ
8
• MEASURED FIELD — THEORETICAL INDUCED FIELD FOR B_T = 9γ, M = 1.0 x 10^{20} cgs
B_X
+11
+9
+7
B_Y
+2
0
-2
B_Z
+2
0
-2
SEQUENCE NO.= 111160 180 200 220 240 260 280 111300
19 OCTOBER 1967

FIGURE 8

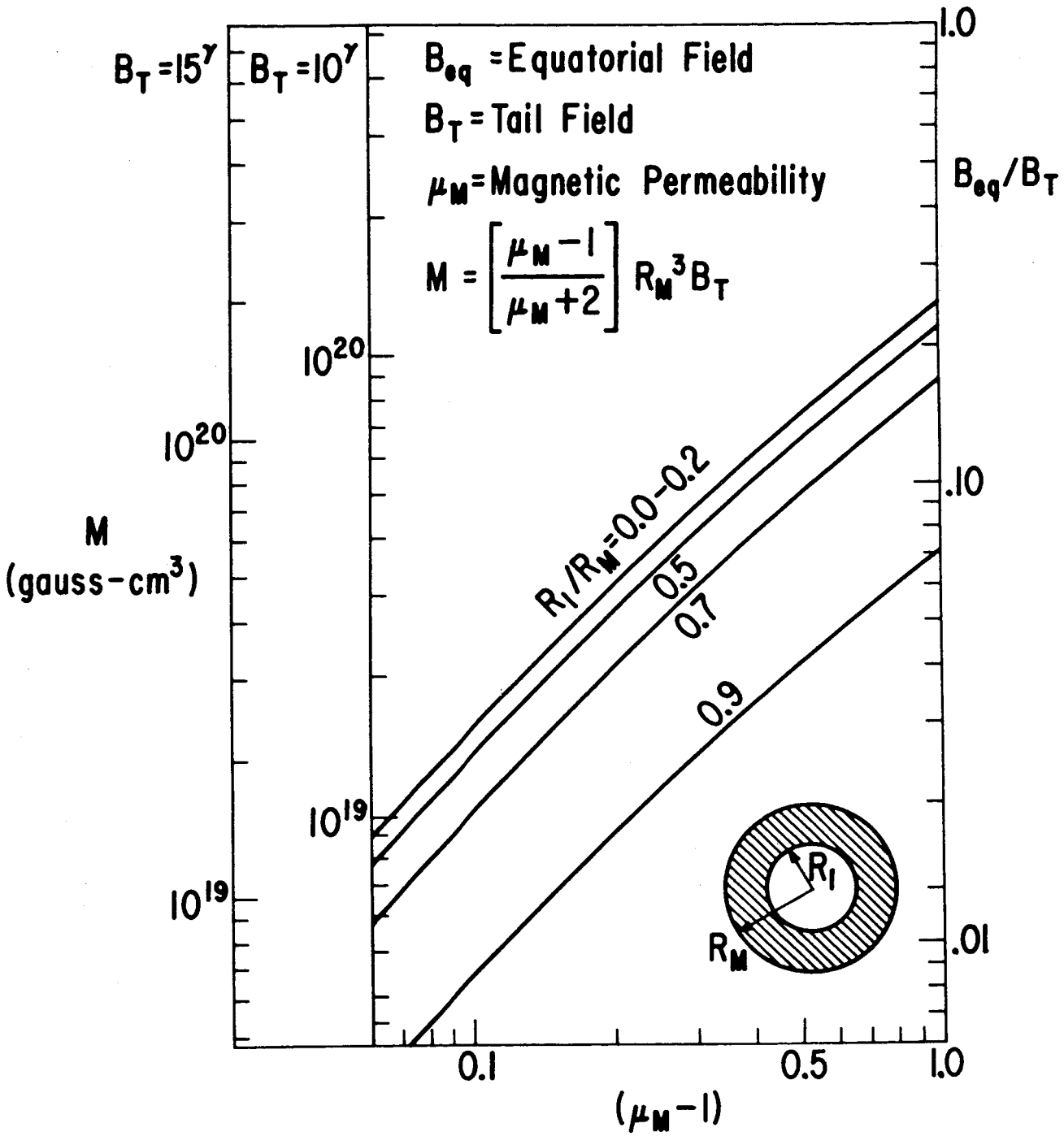
$B_T = 15^\gamma$
$B_T = 10^\gamma$
B_{eq} = Equatorial Field
B_T = Tail Field
μ_M = Magnetic Permeability
$M = \left[\frac{\mu_M - 1}{\mu_M + 2}\right] R_M^3 B_T$
10^{20}
10^{20}
10^{19}
10^{19}
M
(gauss-cm^3)
R_I/R_M=0.0-0.2
0.5
0.7
0.9
R_I
R_M
1.0
.10
.01
B_{eq}/B_T
0.1
0.5
1.0
$(\mu_M - 1)$

FIGURE 9